Nonlinear dressed states at the miscibility-immiscibility threshold

E. Nicklas, W. Muessel, H. Strobel, P. G. Kevrekidis, and M. K. Oberthaler

Phys. Rev. A **92**, 053614 — Published 17 November 2015

DOI: 10.1103/PhysRevA.92.053614

Nonlinear dressed states at the miscibility-immiscibility threshold

E. Nicklas[1], W. Muessel[1], H. Strobel[1], P.G. Kevrekidis[1,2], M.K. Oberthaler[1]
[1] *Kirchhoff-Institut für Physik, Universität Heidelberg, Im Neuenheimer Feld 227, 69120 Heidelberg, Germany*
[2] *Department of Mathematics and Statistics, University of Massachusetts, Amherst MA 01003-4515, USA*

The dynamical evolution of spatial patterns in a complex system can reveal the underlying structure and stability of stationary states. As a model system we employ a two-component Bose-Einstein condensate at the transition from miscible to immiscible with the additional control of linear interconversion. Excellent agreement is found between the detailed experimental time evolution and the corresponding numerical mean-field computations. Analysing the dynamics of the system, we find clear indications of stationary states that we term nonlinear dressed states. A steady state bifurcation analysis reveals a smooth connection of these states with dark-bright soliton solutions of the integrable two-component Manakov model.

Bose-Einstein condensates have been established over the past two decades as a prototypical testbed for exciting developments ranging from nonlinear dynamics and wave phenomena to superfluid features and quantum phase transitions [1–5]. Especially two-component ultracold gases are ideal for the study of the connection of topological solutions of integrable systems and their variants in the presence of different types of perturbations [6, 7]. Identification and exploration of the topological stationary nonlinear solutions in complex systems can give essential insight into the ongoing physics. We report here on the finding as well as experimental detection of a new class of nonlinear stationary states in two component systems with linear interconversion at the threshold between miscibility and immiscibility.

The properties of multi-component Bose Einstein condensates have been studied in numerous contexts. In particular, early experimental efforts produced binary mixtures of two different hyperfine states of ^{23}Na [8] and of ^{87}Rb [9]. The progressively improving experimental control has enabled detailed observations of phase separation phenomena and associated multi-component dynamics [10–16]. More recently, the mixing-demixing dynamics has been controlled both in pseudo-spinor (two-component) [17] and spinor systems [18] via external coupling fields. As a result, formation of domain walls has been observed. In these systems additional topological excitations such as dark-bright solitons do exist. These have been experimentally realized building on dynamical instabilities present in the regime of two counterflowing superfluids [7]. The ability of phase imprinting offers a controlled path for the generation of individual such topological states [6]. All these observations are adequately captured by the mean-field description. Thus, the well established integrable Manakov model [19], i.e. two nonlinearly interacting classical fields in one dimension at the miscibility-immiscibility threshold, forms a basis for understanding the corresponding characteristics. This model is also examined in other physical systems such as nonlinear polarization optics where multiple dark-bright and dark-dark soliton solutions can be systematically constructed [20].

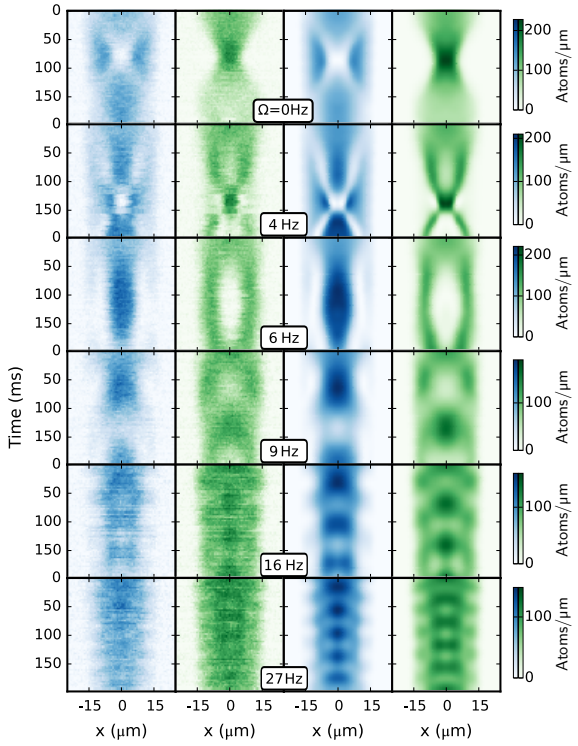

FIG. 1. (Color online) Comparison of observed and numerically calculated time dynamics of an elongated two component condensate in the presence of a dressing field of different amplitudes Ω. The asymmetry in the intra-species scattering lengths pushes component $|1\rangle$ to the wings of the trap for $\Omega = 0$. The trend reverses for $\Omega = 2\pi \times 6\,\mathrm{Hz}$. As Ω increases further, the amplitude of the oscillatory dynamics decreases and in the large coupling limit the system is well approximated by stationary dressed states.

Here, we study the nonlinear dynamics of a two-component Bose gas at the transition from miscible to immiscible, arising through linear interconversion between the two components. In particular, we utilize a Rabi coupling between two hyperfine states of ^{87}Rb and identify its significant impact on the dynamics as shown in Fig. 1.

The comparison of experimental results with theoretical predictions shows excellent agreement. A more systematic analysis discussed below reveals that these observations can be understood as a consequence of the presence of stable nonlinear stationary states. These we will term "nonlinear dressed states" (NDS). Additionally, this new class of states is found to be interconnected as a function of the linear coupling strength via a series of Hamiltonian saddle-node, as well as Hopf bifurcations [21]. A key observation is that the resulting rich bifurcation diagram connects the NDS with two previously studied limits. For vanishing linear coupling we recover the sequence of dark-bright solitonic states of the integrable Manakov model [20] and in the limit of dominating interconversion we identify the known dressed states in the homogeneous miscible regime [22].

In our experiment we initially prepare the gas in a product of single particle dressed states, i.e. an equal superposition of the two components, for given Rabi coupling strength characterized by $\Omega_0 = 2\pi \times 600\,\mathrm{Hz}$. This is achieved by realizing a fast $\pi/2$ pulse with strong coupling and a subsequent phase-adjusted driving (with phase $\phi = -\pi/2$) at the coupling strength of interest. It is important to note that with this procedure the higher excited states of the system are prepared. Fig. 1 illustrates the comparison of the spatial dynamics for the two components, after a quench to different values of Ω. The theoretical dynamics is based on the non-polynomial Schrödinger equation (NPSE, see Appendix) [23]. This confirms the relevance of the mean-field model as a suitable tool for predicting the dynamics.

We observe that for $\Omega = 0$, i.e. no linear coupling, component $|1\rangle$ is pushed to the edge of the condensate. This results from the fact that the repulsive interaction of component $|1\rangle$ is larger than for the other component $a_{11} > a_{22}$ ($[a_{11}, a_{22}, a_{12}] = [100.4, 95.0, 97.7]a_{\mathrm{Bohr}}$ [12, 24]; see, however, also [25]); here, a_{xy} represents the scattering length between the x, y components. It is important to note that this is not due to demixing dynamics resulting from an instability corresponding to $\Delta < 1$ (although in our case $\Delta < 1$, its proximity to unity is such that the growth times of the most unstable modes are much longer than the time scale of our experiments). Instead, it has to be regarded as energetic separation of the two components. For the experiment described here, $\Delta = a_{11}a_{22}/a_{12}^2 = 0.998(2) \approx 1$. This trend is *reversed* as Ω is increased, where the more strongly interacting component $|1\rangle$ is compressed during the dynamics initiated by the quench (see Fig. 1 for $\Omega = 2\pi \times 6\,\mathrm{Hz}$). This is a consequence of the finite size of the system and is well captured by the numerical calculations. For higher values of linear coupling we observe faster oscillatory dynamics which on average is reminiscent of the strongly dressed state regime [22] reported in the context of miscibility control by linear interconversion [17].

Before bringing these results into a more general context we briefly discuss the experimental and numerical methods used to monitor the system at hand. We create a Bose-Einstein condensate of 5600 ^{87}Rb atoms in an elongated optical dipole trap with a longitudinal trap frequency $\omega_x = 2\pi \times 23.4\,\mathrm{Hz}$ and a transverse confinement of $\omega_\perp = 2\pi \times 490\,\mathrm{Hz}$. The atoms are initially in state $|1\rangle = |F = 1, m_F = -1\rangle$ of the ground state hyperfine manifold and can be linearly coupled to state $|2\rangle = |F = 2, m_F = 1\rangle$ via two-photon microwave and radio frequency radiation. The detuning from the intermediate $|2, 0\rangle$ level is $-2\pi \times 200$ kHz. A fast $\Omega\tau = \pi/2$ pulse with $\Omega = 2\pi \times 600\,\mathrm{Hz}$ creates a spatially homogeneous equal superposition of the two states. Within 5 μs the phase of the coupling field is changed by $-\pi/2$ and the amplitude is reduced to realize coupling strengths in the range $0 < \Omega < 2\pi \times 60$ Hz. A uniform magnetic field $B = 3.23\,\mathrm{G}$ guarantees that the differential Zeeman shift between states $|1\rangle$ and $|2\rangle$ is equal to second order and the influence of magnetic field fluctuations is minimized. The mean field shift due to the different intra-species scattering lengths $a_{11} \neq a_{22}$ is compensated with a detuning of $\delta = -2\pi \times 16\,\mathrm{Hz}$, which is adjusted through the frequency of the rf coupling field. The time evolution is obtained by repeating this procedure and detecting the atomic distributions after different evolution times past the initial $\pi/2$ pulse using state-selective absorption imaging with a spatial resolution of 1.1 μm.

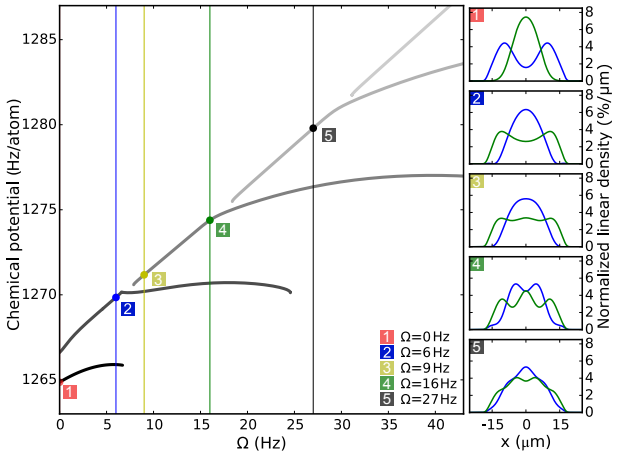

FIG. 2. (Color online) Stationary states in the presence of a linear coupling field, exhibiting an intriguing cascade of branches. The right columns show the theoretically obtained normalized density profiles for the two components $|1\rangle$ (blue) and $|2\rangle$ (green) for five characteristic values corresponding to the parameters of Fig. 1.

Our quantitative theoretical analysis is based on both a study of the system's time evolution and on the exploration of its stationary states and their Bogoliubov-de Gennes stability analysis (see Appendix). The time evolution of the linearly coupled atomic clouds is performed via the NPSE [23]. The simulation is initialized with the mean field ground state of $N = 5600$ atoms in state $|1\rangle$ calculated via a Newton scheme. It subsequently replicates the experimental procedure described above. For the dynamical evolution in Figure 1, we have also incor-

porated in the NPSE two- and three-body losses where the most important contribution comes from the spin relaxation loss of $F = 2$.

To shed light on the complex sequence of dynamical features observed for different values of Ω, we proceed to compute the stationary states of the coupled NPSE system in Fig. 2. These are obtained by means of a fixed point (Newton) method as detailed in the appendix, which is capable of also capturing dynamically unstable states, a feature critical to our discussion below. The stationary solutions are constructed by means of a small change to the parameter Ω, using the previously converged stationary state as a seed. This parametric continuation approach reveals a sequence of branches which appear to be disconnected from each other, as can be seen in Fig. 2. These form part of a progression whereby an increasing number of spatial density modulations (and number of maxima) of each component is present in each higher branch; see Fig. 2(b). Notice, in particular, how component $|2\rangle$ evolves from single hump for vanishing Ω (top panel of Fig. 2(b)) to double and multi-humped as Ω is increasing.

We now show that these stationary states are intimately connected to the averaging of the experimental and numerical dynamical observations, as is illustrated in Fig. 3. For comparison, the population differences of the components are averaged over the respective period of the temporal evolution. Fig. 3(a) represents the experimental observations, panel (b) the direct numerical time dynamics (via the NPSE) while panel (c) depicts the corresponding stationary stable nonlinear dressed states; see also the discussion below. We find excellent agreement between time-averaged NPSE and the stationary NDS state predictions. Only slight asymmetries (plausibly due to inhomogeneities of the coupling field) can be detected in these rows. These are roughly the same in all rows in absolute magnitude but in our density difference diagnostic they become more pronounced when the densities are nearly equal (i.e., in rows 4 and 5). If the dynamics can be understood as interference between different non-linear stationary states where one is much more populated than the others, time averaging would reveal the most populated state since the rest would average to zero in the long time limit.

In accordance with bifurcation theory, the depicted endpoints for our stationary solutions (see Fig. 2) cannot be isolated, but rather have to be continued. To reveal this structure we utilize the method of pseudo-arclength continuation [26] enabling the continuation of the branches around these apparent endpoints. For this analysis we employed the one dimensional Gross-Pitaevskii equation to facilitate the stability computations, yet the qualitative observations reported below are unaffected by this. Corresponding results including the spatial profile at selected points along one branch are shown in Fig. 4. This illustrates that the nonlinear dressed states are smoothly connected to solutions of the dark-bright soliton type for vanishing Ω that are known

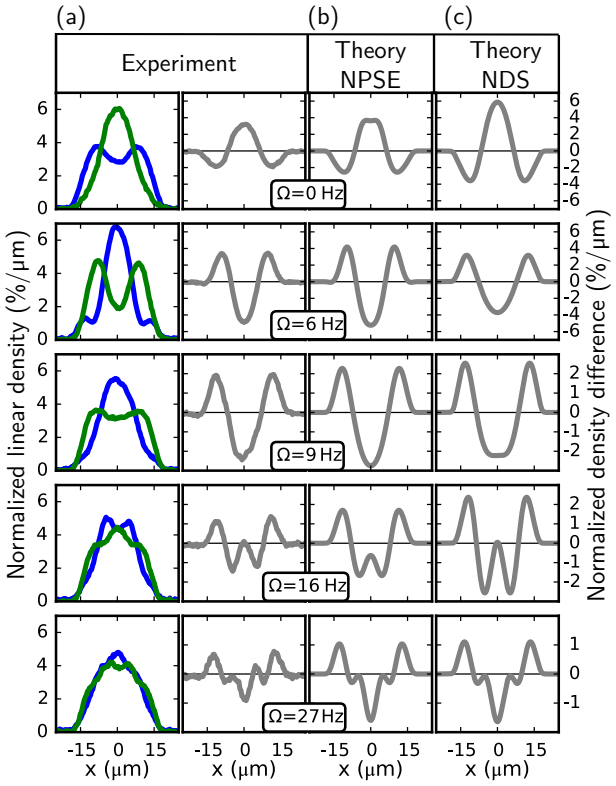

FIG. 3. (Color online) Detailed comparison of the time-averaged density difference profiles with the stationary states. (a) We extract the time averaged density profiles from the experimentally observed dynamics shown in Fig. 1, averaging over full oscillation periods for each value of Ω and normalizing the averaged profile (see Appendix), as shown in the left column. The difference of the time-averaged density profiles in the experiment is shown in the right column. (b) The same procedure is repeated for the numerical simulations of the NPSE and in (c) compared to the stationary states from Fig. 2 for the respective values of Ω, i.e., the NDS. The qualitative agreement reveals that the time averaged profiles are accurately captured by the corresponding stationary nonlinear dressed states. On a quantitative level, differences remain, as the dissipative mechanisms are not accounted for in the determination of the NDS.

to exist in the context of the Manakov model [20]. The highlighted branch in Fig. 4 connects the state consisting of eight topological excitations to the one with ten; similar features arise for lower, as well as for higher branches (with correspondingly lower and higher soliton multiplicities). The symmetry of our initial guess selects the states with an even number of excitations. The observed pattern in the experiment corresponds to the segment of the branch between the panels 2 and 3 in Fig. 4. The numerical Bogoliubov-de Gennes (linearization) stability analysis confirms that this segment is stable. The stability regime is delimited by a saddle node bifurcation at the lower corner (see e.g. marker 3 in Fig. 4). This is characterized by a turning point of the branch connected with a zero crossing of an eigenfrequency in the

Bogoliubov-de Gennes analysis. The upper limit of the stability segment (see e.g. marker 4 in Fig. 4) is associated with a Hamiltonian Hopf bifurcation [21], whereby quartets of eigenfrequencies emerge and destabilize the branch. Both unstable parts of the branch connect in the limit of $\Omega = 0$ to a train of dark-bright solitons but with different even multiplicity. We emphasize that the stable stationary solutions naturally connect to the linear dressed states in the limit of large Ω [22]. The amplitude of the spatial structure as well as its length scale decreases as Ω approaches this limit in accordance with the Bogoliubov-de Gennes analysis of the uniform state [27].

We note that for small linear couplings both the profile and the energy is strongly influenced by the finite size of the system. Especially the observed interchange of the components between $\Omega = 2\pi \times 4\,\mathrm{Hz}$ and $\Omega = 2\pi \times 6\,\mathrm{Hz}$ (see Fig. 1) can be attributed to the turning point of the lowest branch shown in Fig. 4. The lower two branches in Fig. 4 represent solutions whose spatial extent (even with a single hump) induces competition with the spatial length allowed by the trap, hence their "unusual" shape.

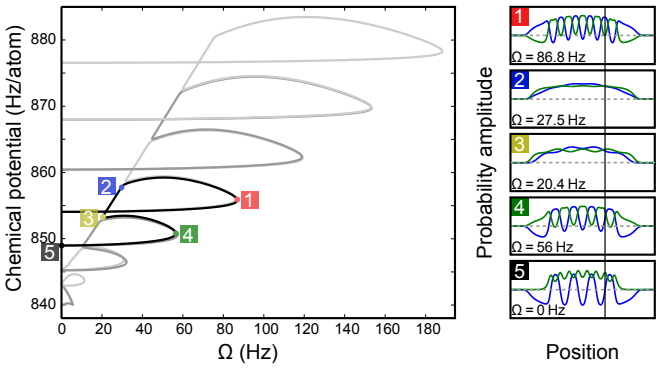

FIG. 4. (Color online) The bifurcation loop structure for the stationary states. The left graph shows the chemical potential of the stationary states as a function of the linear coupling. The states are stable only along the linear parts, e.g. between markers 2 and 3, while the loops are unstable. The graphs at the right illustrate the spatial structure of the probability amplitudes of the corresponding stationary states. Following one specific loop we find that the nonlinear dressed states are smoothly connected to dark-bright soliton trains at $\Omega = 0$ characterized by zero crossings of one component and a corresponding amplitude maximum for the other component. The location of one of the dark-bright solitons in the state identified by marker 5 is indicated by the vertical line. Within each branch two additional topological excitations are added as the energy increases.

In the present work, we have studied experimentally and theoretically the extension of the Manakov model by introducing linear coupling between the two components. In the numerical computations emulating the experiment, we also incorporate the relevant nonlinear losses and obtain quantitative agreement between the two. We find stable stationary solutions for any value of the linear coupling which we term nonlinear dressed states. The theoretical identification is found to be in excellent agreement with our experimenal observations. Furthermore, we establish a connection to limiting solutions in the form of dark-bright soliton trains in the vanishing linear coupling limit and to linear dressed states in the large coupling limit. The associated branches reveal stable and unstable segments separated by saddle-node and Hamiltonian Hopf bifurcations.

Our results reveal a previously unidentified connection between highly nonlinear stationary states and the weakly interacting regimes reached via a controlled perturbation. Identifying the nature of perturbations leading to such a smooth connection may provide critical insights into a physical system revealing universal characteristics for highly excited states. The translation of our findings to spin models, e.g. in our case the mapping to a transverse Heisenberg model [28], can prove fruitful in characterizing the high energy part of the excitation spectrum. This might have consequences on the recently discussed excited state quantum phase transitions [29]. Moreover, it would be interesting to explore how such phenomenologies may extend to higher dimensional settings, potentially forming a multi-dimensional analog of nonlinear dressed states and a set of branches connecting different spatially modulated states.

The authors acknowledge experimental contributions by Jiří Tomkovič and fruitful discussions with Boris Malomed. This work was supported by the Heidelberg Center for Quantum Dynamics and the European Commission small or medium-scale focused research project QIBEC (Quantum Interferometry with Bose-Einstein condensates, Contract Nr. 284584). W.M. acknowledges support by the Studienstiftung des deutschen Volkes. P.G.K. acknowledges support from the National Science Foundation under grant DMS-1312856, and from the US-AFOSR under grant FA9550-12-10332.

APPENDIX

A. Extraction of the linear density profiles

The two components are detected via state-selective high-intensity absorption imaging with a pulse duration of $\tau = 10\,\mu$s, using two subsequent pulses which are temporally separated by $780\,\mu$s. The obtained two-dimensional density distributions are integrated along the short axis of the atomic cloud to obtain the longitudinal linear density profiles. Due to the destructive nature of absorption imaging, the experiment is repeated with different evolution times.

For the time-averaged profiles, the linear density profiles of each component are averaged over full oscillation periods. To compensate spurious population differences caused by the small differences of the detectivities for the two states, the individual averaged profiles are normalized. To ensure comparability, the same procedure is applied to the theoretical time-averaged profiles.

B. Non-polynomial Schrödinger equation

In the non-polynomial Schrödinger equation, the ansatz for the order parameter of the BEC in a close to one-dimensional situation is

$$\Psi_k(x,y,z,t) = \frac{1}{\sqrt{\pi}a_\perp\sigma_k(x,t)}\exp\left\{-\frac{y^2+z^2}{2(a_\perp\sigma_k(x,t))^2}\right\}\psi_k(x,t), \tag{1}$$

where $\sigma_k(x,t)$ describe the transversal extension relative to the harmonic oscillator length $a_\perp = \sqrt{\hbar/m\omega_\perp}$. The longitudinal parts ψ_k are normalized on the number of atoms in each component: $\int|\psi_k(x,t)|^2\mathrm{d}x = N_k(t)$. This turns the coupled three-dimensional Gross-Pitaevskii equations (GPE) into the coupled set

$$\mathrm{i}\hbar\partial_t\psi_1 = \left[\mathcal{H}_0 + \frac{\hbar\omega_\perp}{2}\frac{1+\sigma_1^4}{\sigma_1^2} + \frac{\mathcal{G}_{11}}{\sigma_1^2}|\psi_1|^2 + \frac{2\mathcal{G}_{12}}{\sigma_1^2+\sigma_2^2}|\psi_2|^2 + \frac{\mathcal{G}_{111}}{\sigma_1^4}|\psi_1|^4 + \frac{\hbar\delta}{2}\right]\psi_1 + \frac{\hbar\Omega}{2}\psi_2 + \mathcal{G}_1 \tag{2}$$

$$\mathrm{i}\hbar\partial_t\psi_2 = \left[\mathcal{H}_0 + \frac{\hbar\omega_\perp}{2}\frac{1+\sigma_2^4}{\sigma_2^2} + \frac{\mathcal{G}_{22}}{\sigma_2^2}|\psi_2|^2 + \frac{2\mathcal{G}_{12}}{\sigma_1^2+\sigma_2^2}|\psi_1|^2 + \frac{\mathcal{G}_{222}}{\sigma_2^4}|\psi_2|^4 - \frac{\hbar\delta}{2}\right]\psi_2 + \frac{\hbar\Omega^*}{2}\psi_1 + \mathcal{G}_2 \tag{3}$$

$$\tag{4}$$

and

$$\sigma_1^4 = 1 + 2a_{11}|\psi_1|^2 + 8a_{12}|\psi_2|^2\frac{\sigma_1^4}{(\sigma_1^2+\sigma_2^2)^2}, \tag{5}$$

$$\sigma_2^4 = 1 + 2a_{22}|\psi_2|^2 + 8a_{12}|\psi_1|^2\frac{\sigma_2^4}{(\sigma_1^2+\sigma_2^2)^2}. \tag{6}$$

The term $\mathcal{H}_0 = -\hbar^2\partial_x^2/2m + m\omega_x^2x^2/2$ contains the kinetic energy and the spin-independent longitudinal trapping potential, and $\mathcal{G}_{jk} = (g_{jk} - \mathrm{i}\hbar K_2^{(jk)}/2)/(2\pi a_\perp^2)$ describe two-body interactions $g_{jk} = (4\pi\hbar^2/m)a_{jk}$ with the s-wave scattering lengths a_{jk} and two-body loss channels with the loss coefficients $K_2^{(jk)}$. $\mathcal{G}_j = (-\mathrm{i}\hbar K_1^{(j)}/2)$ describe one-body losses and $\mathcal{G}_{jjj} = (-\mathrm{i}\hbar K_3^{(jjj)}/2)/(2\pi a_\perp^2)^2$ capture three-body losses. $\Omega = \Omega_0\exp(\mathrm{i}\phi)$ is the phase controlled linear Rabi coupling with detuning δ from atomic resonance.

For constant transversal width $\sigma_k = 1$, the NPSEs turn into the corresponding 1DGPEs. For both approaches, the stationary solutions for the ansatz $\psi_k(x,t) = \exp(-\mathrm{i}\mu_k t)\psi_k(x,0)$ with the chemical potentials μ_k are obtained on a linear grid. The time evolution is calculated with a 4th order Runge-Kutta method.
The employed loss parameters in the simulations are $K_1^{(1)} = K_1^{(2)} = 0.01\,\mathrm{s}^{-1}$, $K_2^{(22)} = 2.39\times10^{-14}\,\mathrm{cm}^3/\mathrm{s}$, $K_2^{(12)} = 3.9\times10^{-14}\,\mathrm{cm}^3/\mathrm{s}$, $K_3^{(111)} = K_3^{(222)} = 5.8\times10^{-30}\,\mathrm{cm}^6/\mathrm{s}$ with all others set to zero.

C. Newton's method

For obtaining stationary states of either NPSE or 1DGPE, Newton's method is employed. It converges quadratically to any stationary solution if the initial guess for the wave functions is sufficiently close to the stationary state, and thus can capture not only just the ground state, as is the case for the often employed evolution in imaginary time. The stationary equations are

$$\begin{pmatrix} H_{11} & H_{12} \\ H_{21} & H_{22}\end{pmatrix}\begin{pmatrix}\psi_1\\ \psi_2\end{pmatrix} = \begin{pmatrix}\mu_1\psi_1\\ \mu_2\psi_2\end{pmatrix}. \tag{7}$$

Both ψ_1 and ψ_2 are realized on the grid with spacing Δx and are thus vectors $(\psi_k)_j$ with n_g entries. All loss constants and the detuning δ are set to zero for this steady state computation. For the Newton method, the normalization conditions $\sum_j(\psi_k)_j^2 = N_k$ are introduced via Lagrange multipliers λ_k, assuming that the solutions ψ_k are real. This leads to a system of equations for the $2n_g+2$ variables $\Phi = \{\psi_1,\psi_2,\lambda_1,\lambda_2\}$, which reads

$$F(\Phi) = \begin{pmatrix} \begin{pmatrix} H_{11}-\mu_1 & H_{12} \\ H_{21} & H_{22}-\mu_2\end{pmatrix}\begin{pmatrix}\psi_1\\ \psi_2\end{pmatrix} + \begin{pmatrix}2\lambda_1\Delta x\psi_1\\ 2\lambda_2\Delta x\psi_2\end{pmatrix} \\ \sum_j(\psi_1)_j^2\Delta x - N_1 \\ \sum_j(\psi_2)_j^2\Delta x - N_2 \end{pmatrix} = 0. \tag{8}$$

Newton's iterative method for finding the nearest root for a given starting point Φ^0 of this equation reads

$$\Phi^{k+1} = \Phi^k - J^{-1}(\Phi^k)F(\Phi^k). \tag{9}$$

Computing the inverse of the Jacobian $J_{ij}(\Phi) = \partial F_i/\partial \Phi_j$ in every step is the computationally most expensive part.

D. Bogoliubov-de Gennes stability analysis

The BdG analysis is a method for numerically computing the excitation spectrum and the corresponding spatial modes on top of a background state of the two stationary order parameters. We assume $\psi_{k,0}(x)$ to be a known stationary solution of the NPSE with the time evolution $\psi_{k,0}(x,t) = \exp(-\mathrm{i}\mu_k t)\psi_{k,0}(x,0)$ and $\delta\psi_k(x,t)$ a perturbation on top of $\psi_{k,0}(x,0)$

$$\psi_{k,0}(x,t) = \exp(-\mathrm{i}\mu_k t)[\psi_{k,0}(x,0) + \epsilon\,\delta\psi_k(x,t)]$$

with $\epsilon \ll 1$. Inserting this state into the time-dependent NPSE and ignoring terms of second or higher order in ϵ results in equations of motion for the perturbations $\delta\psi_k(x,t)$. We assume them to be of the form

$$\delta\psi_k(x,t) = a_k(x)e^{\mathrm{i}\omega t} + b_k^*(x)e^{-\mathrm{i}\omega t}$$

with the complex amplitudes $a_k(x)$ and $b_k(x)$ and the energy $\hbar\omega$. Inserting this ansatz into the equations of motion and sorting by $e^{-i\omega t}$ and $e^{i\omega t}$ results in four coupled equations for the excitation modes

$$\hbar\omega \begin{pmatrix} a_1 \\ b_1 \\ a_2 \\ b_2 \end{pmatrix} = \begin{pmatrix} A_1 & B_1 & A_{12} & B_{12} \\ -B_1^* & -A_1^* & -B_{12}^* & -A_{12}^* \\ A_{12} & B_{12} & A_2 & B_2 \\ -B_{12}^* & -A_{12}^* & -B_2^* & -A_2^* \end{pmatrix} \begin{pmatrix} a_1 \\ b_1 \\ a_2 \\ b_2 \end{pmatrix}$$

with the matrix elements

$$\begin{aligned}
A_1 &= \mathcal{H}_0 + \frac{\hbar\omega_\perp}{2}\frac{1+\sigma_1^4}{\sigma_1^2} + \frac{2\mathcal{G}_{11}}{\sigma_1^2}|\psi_{1,0}|^2 + \frac{2\mathcal{G}_{12}}{\sigma_1^2+\sigma_2^2}|\psi_{2,0}|^2 + \frac{\hbar\delta}{2} - \mu_1 \\
A_2 &= \mathcal{H}_0 + \frac{\hbar\omega_\perp}{2}\frac{1+\sigma_2^4}{\sigma_2^2} + \frac{2\mathcal{G}_{22}}{\sigma_2^2}|\psi_{2,0}|^2 + \frac{2\mathcal{G}_{12}}{\sigma_1^2+\sigma_2^2}|\psi_{1,0}|^2 - \frac{\hbar\delta}{2} - \mu_2 \\
B_1 &= \frac{\mathcal{G}_{11}}{\sigma_1^2}|\psi_{1,0}|^2 \\
B_2 &= \frac{\mathcal{G}_{22}}{\sigma_2^2}|\psi_{2,0}|^2 \\
A_{12} &= \frac{2\mathcal{G}_{12}}{\sigma_1^2+\sigma_2^2}\psi_{1,0}^*\psi_{2,0} + \frac{\hbar\Omega}{2} \\
B_{12} &= \frac{2\mathcal{G}_{12}}{\sigma_1^2+\sigma_2^2}\psi_{1,0}^*\psi_{2,0}
\end{aligned}$$

The eigenmodes and eigenvectors of the matrix are obtained on the linear grid by numerical diagonalization. Here, all loss constants and the detuning δ are set to zero, as in the search for the stationary states with Newton's method (i.e., we consider the corresponding Hamiltonian problem). Due to the Hamiltonian structure of the underlying model, the stability of the nonlinear dressed states of either NPSE or 1DGPE is confirmed if no BdG excitation mode obtains an imaginary part above the numerical accuracy.

[1] C. J. Pethick and H. S. Smith, *Bose-Einstein Condensation in Dilute Gases*, Cambridge University Press, Cambridge, 2002.

[2] L.P. Pitaevskii and S. Stringari, *Bose-Einstein Condensation*, Oxford University Press (Oxford, 2003).

[3] P.G. Kevrekidis, D.J. Frantzeskakis, and R. Carretero-González (eds.), *Emergent nonlinear phenomena in*

Bose-Einstein condensates. Theory and experiment (Springer-Verlag, Berlin, 2008).

[4] L.D. Carr, *Understanding Quantum Phase Transitions*, (Taylor & Francis, Boca Raton, 2010).

[5] N. Proukakis, S. Gardiner, M. Davis, M. Szymanska, *Quantum gases: finite temperature and non-equilibrium dynamics*, (Imperial College Press, London, 2013).

[6] C. Becker, S. Stellmer, P. Soltan-Panahi, S. Dorscher, M. Baumert, E. M. Richter, J. Kronjäger, K. Bongs, and K. Sengstock, Nat. Phys. **4**, 496 (2008).

[7] C. Hamner, J.J. Chang, P. Engels, and M. A. Hoefer, Phys. Rev. Lett. **106**, 065302 (2011); M.A. Hoefer, J.J. Chang, C. Hamner, and P. Engels, Phys. Rev. A **84**, 041605 (2011); D. Yan, J.J. Chang, C. Hamner, P.G. Kevrekidis, P. Engels, V. Achilleos, D. J. Frantzeskakis, R. Carretero-Gonzalez, P. Schmelcher, Phys. Rev. A **84**, 053630 (2011); D. Yan, J.J. Chang, C. Hamner, M. Hoefer, P.G. Kevrekidis, P. Engels, V. Achilleos, D.J. Frantzeskakis and J. Cuevas, J. Phys. B: At. Mol. Opt. Phys., **45** 115301 (2012).

[8] D.M. Stamper-Kurn, M. R. Andrews, A. P. Chikkatur, S. Inouye, H.-J. Miesner, J. Stenger, and W. Ketterle, Phys. Rev. Lett. **80**, 2027 (1998).

[9] D.S. Hall, M.R. Matthews, J.R. Ensher, C.E. Wieman, and E.A. Cornell, Phys. Rev. Lett. **81**, 1539 (1998).

[10] J. Stenger, S. Inouye, D.M. Stamper-Kurn, H.-J. Miesner, A.P. Chikkatur and W. Ketterle, Nature **396**, 345 (1998).

[11] V. Schweikhard, I. Coddington, P. Engels, S. Tung and E.A. Cornell, Phys. Rev. Lett. **93**, 210403 (2004).

[12] K.M. Mertes, J.W. Merrill, R. Carretero-González, D.J. Frantzeskakis, P.G. Kevrekidis and D.S. Hall, Phys. Rev. Lett. **99**, 190402 (2007).

[13] S.B. Papp, J.M. Pino and C.E. Wieman, Phys. Rev. Lett. **101**, 040402 (2008).

[14] R.P. Anderson, C. Ticknor, A.I. Sidorov, B.V. Hall, Phys. Rev. A **80**, 023603 (2009).

[15] M. Egorov, B. Opanchuk, P. Drummond, B. V. Hall, P. Hannaford, and A. I. Sidorov Phys. Rev. A **87**, 053614 (2013).

[16] S.Tojo, Y. Taguchi, Y. Masuyama, T. Hayashi, H. Saito and T. Hirano, Phys. Rev. A **82**, 033609 (2010).

[17] E. Nicklas, H. Strobel, T. Zibold, C. Gross, B.A. Malomed, P.G. Kevrekidis, M.K. Oberthaler, Phys. Rev. Lett. **107**, 193001 (2011).

[18] Y.-J. Lin, K. Jiménez-García, I.B. Spielman, Nature (London) **471**, 83 (2011).

[19] S. V. Manakov, Zh. Eksp. Teor. Fiz. **65**, 505 (1973) [Sov. Phys. JETP **38**, 248 (1973)]; V. E. Zakharov and S. V. Manakov, Zh. Eksp. Teor. Fiz. **71**, 203 (1976) [Sov. Phys. JETP **42**, 842 (1976)]. For a more detailed discussion see e.g. M.J. Ablowitz, B. Prinari and A.D. Trubatch, *Discrete and Continuous Nonlinear Schrödinger Systems*, Cambridge University Press (Cambridge, 2004).

[20] A.P. Sheppard, Yu.S. Kivshar, Phys. Rev. E **55**, 4773 (1997).

[21] See e.g. for a recent discussion R.H. Goodman, J. Phys. A: Math. Theor. **44**, 425101 (2011) and references therein.

[22] C.P. Search and P.R. Berman, Phys. Rev. A **63**, 043612 (2001).

[23] The one component version of the model was derived in L. Salasnich, A. Parola, and L. Reatto, Phys. Rev. A **65**, 043614 (2002), while the two-component version used herein was obtained in L. Salasnich and B. A. Malomed, Phys. Rev. A **74**, 053610 (2006).

[24] A. M. Kaufman, R.P. Anderson, T. M. Hanna, E. Tiesinga, P. S. Julienne, and D. S. Hall, Phys. Rev. A **80**, 050701 (2009).

[25] It should be noted in passing that recent work of M. Egorov, B. Opanchuk, P. Drummond, B. V. Hall, P. Hannaford, and A. I. Sidorov Phys. Rev. A **87**, 053614 (2013) suggests slightly different values for $a_{22} = 95.44 a_{\rm Bohr}$ and $a_{12} = 98.006 a_{\rm Bohr}$ (also A.I. Sidorov, personal communication). Nevertheless, the conclusions presented herein will not be qualitatively affected by such a variation.

[26] E.J. Doedel, *Lecture Notes on Numerical Analysis of Nonlinear Equations*, available at: http://cmvl.cs.concordia.ca/publications.html.

[27] P. Tommasini, E.J.V. de Passos, A.F.R. de Toledo Piza, M.S. Hussein, E. Timmermans, Phys. Rev. A **67**, 023606 (2003).

[28] K. Kasamatsu, M. Tsubota, M. Ueda, Phys. Rev. A **71**, 043611 (2005).

[29] M.A. Caprio, P. Cernar, and F. Iachello, Ann. Phys. (N.Y.) **323**, 1106 (2008).